The Astrophysical Journal Letters, 887:L2 (4pp), 2019 December 10 https://doi.org/10.3847/2041-8213/ab58cf

Heavy Ion Acceleration by Super-Alfvénic Waves

S. Matsukiyo[1], T. Akamizu[2], and T. Hada[1]
[1] Faculty of Engineering Sciences, Kyushu University, Kasuga, Fukuoka, 816-8580, Japan; matsukiy@esst.kyushu-u.ac.jp, hada@esst.kyushu-u.ac.jp
[2] Interdisciplinary Graduate School of Engineering Sciences, Kyushu University, Kasuga, Fukuoka, 816-8580, Japan
Received 2019 October 7; revised 2019 November 17; accepted 2019 November 19; published 2019 December 3

Abstract

A generation mechanism of super-Alfvénic (SPA) waves in multi-ion species plasma is proposed, and the associated heavy ion acceleration process is discussed. The SPA waves are thought to play important roles in particle acceleration since they have large wave electric fields because of their high phase velocity. It is demonstrated by using full particle-in-cell simulations that large amplitude proton cyclotron waves, excited due to proton temperature anisotropy, nonlinearly destabilize SPA waves through parametric decay instability in a three-component plasma composed of electrons, protons, and α particles. At the same time, α cyclotron waves get excited via another decay instability. A pre-accelerated α particle resonates simultaneously with the two daughter waves, the SPA waves and the α cyclotron waves, and it is further accelerated perpendicular to the ambient magnetic field. The process may work in astrophysical environments where a sufficiently large temperature anisotropy of lower mass ions occurs.

Unified Astronomy Thesaurus concepts: Space plasmas (1544); Plasma astrophysics (1261); Interplanetary particle acceleration (826); Solar coronal waves (1995); Alfven waves (23)

1. Introduction

In many space and astrophysical environments observations show that heavy ions are preferentially accelerated. The ratio of galactic cosmic-ray proton flux to helium flux decreases as rigidity increases (Aguilar et al. 2015). An increase of heavy ion abundance is commonly observed in solar energetic particle events (e.g., Klecker et al. 2007; Reames 2017 and the references therein). In situ observations in the terrestrial magnetosphere (e.g., Kronberg et al. 2014 and the references therein) and interplanetary space (Gruesbeck et al. 2015; Dayeh et al. 2017; Filwett et al. 2017) also often detect preferentially accelerated heavy ions. While a number of theories have been proposed, the mechanism of heavy ion acceleration is still under debate. One of the extensively studied processes is resonant wave–particle interactions (see Thorne & Horne 1994, 1993; Horne & Thorne 1997; Gary et al. 2003; Tu et al. 2003; Shevchenko et al. 2006; Wang et al. 2019; and some other earlier works are reviewed in Hollweg & Isenberg 2002).

About two decades ago, Mizuta & Hoshino (2001) proposed a mechanism of preferential acceleration of α particles interacting with two left-hand circularly polarized waves. They showed by performing a test particle simulation that an α particle is efficiently accelerated perpendicular to the ambient magnetic field if one of the two waves is on the branch of super-Alfvénic (SPA) waves in a three-component plasma consisting of electrons, protons, and α particles. In the three-component plasma there are two ion cyclotron wave branches in $\omega-k$ space as shown by the black solid lines in Figure 1, i.e., proton cyclotron waves (upper branch) and α cyclotron waves (lower branch). The SPA waves are the high phase velocity, or small wavenumber, part of the proton cyclotron waves. Although the mechanism proposed by Mizuta & Hoshino (2001) is efficient, this acceleration mechanism has not been paid much attention so far. It is probably because a generation mechanism of the SPA waves has been unclear.

In this study we propose a generation mechanism of the SPA waves through the nonlinear evolution of large amplitude lower phase velocity proton cyclotron waves. The latter waves are easily driven by proton temperature anisotropy known as the electromagnetic ion cyclotron (EMIC) instability. Here, we call this proton EMIC instability. It is confirmed/expected that the anisotropy of the proton temperature often becomes extremely high, $T_{p\perp}/T_{p\parallel} \gg 1$, in circumstances such as a solar coronal hole (Markovskii 2007; Isenberg et al. 2019), high Mach number perpendicular shock front (Sckopke et al. 1983; Shimada & Hoshino 2005), intracluster medium (Santos-Lima et al. 2014), and so on. Here, $T_{p\perp}$ and $T_{p\parallel}$ denote proton temperature perpendicular and parallel to the ambient magnetic field, respectively. The linear growth rate of the proton EMIC instability in sufficiently large anisotropy is obtained as $\gamma \approx (\beta_{p\perp}/2)^{1/2}\Omega_p$, where $\beta_{p\perp}$ is perpendicular proton beta, the ratio of proton pressure perpendicular to the ambient magnetic field to magnetic pressure, and Ω_p denotes proton cyclotron frequency (Davidson & Ogden 1975). Therefore, if $\beta_{p\perp}$ becomes of the order of 0.1 or even higher, very strong proton EMIC instability is expected to be generated. In a nonlinear stage of such strong proton EMIC instability large amplitude proton EMIC waves can be the source of wave–wave interactions. By performing a full particle-in-cell (PIC) simulation, it is shown that the SPA waves are self-consistently generated in the late stage of the proton EMIC instability. We further demonstrate that α particles are preferentially accelerated in the simulation through the process discussed by Mizuta & Hoshino (2001).

2. Nonlinear Generation of Super-Alfvénic Waves

We propose a parametric instability of a proton EMIC wave as a mechanism of SPA wave generation. If once large amplitude proton EMIC waves get excited, they can be a source of parametric instabilities. The lowest-order parametric instability occurs through three wave interactions in which the resonance conditions, $\omega_3 = \omega_1 \pm \omega_2$, $k_3 = k_1 \pm k_2$, are

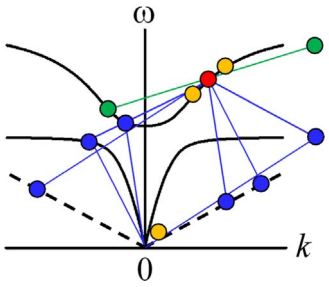

Figure 1. Schematic $\omega-k$ diagram of a number of channels of parametric instabilities in a three-species plasma.

fulfilled among the interacting waves. Here, $\omega_{1,2,3}$ and $k_{1,2,3}$ are the frequencies and wavenumbers of the waves. In a three-component electron–proton-α plasma many channels of parametric instabilities exist. Figure 1 schematically indicates possible channels of parametric instabilities in an $\omega-k$ diagram, when a parent proton EMIC wave (denoted by a red circle) and all daughter waves propagate along the ambient magnetic field. (Note that if the parent wave is on the same branch with negative k, all daughter waves have wavenumbers with opposite signs.) In addition to the two transverse wave branches (proton and α cyclotron waves), a longitudinal wave branch (ion acoustic waves) is denoted by the dashed line. For example, the yellow circles are the possible daughter waves generated due to a modulational instability. The green circles are other possible daughter waves due to a beat instability. In addition, a number of decay instabilities can possibly be generated. In the figure three channels of decay instability are represented by the blue parallelograms. (The above-mentioned resonance conditions lead to the parallelograms in the $\omega-k$ space.) One of them has a daughter wave on the proton cyclotron branch. This daughter wave has a rather small wavenumber and its phase velocity exceeds the Alfvén velocity, i.e., SPA wave. This channel of decay instability was found by Gomberoff et al. (1995) in their linear dispersion analysis. We will see that this channel of decay instability is generated in the nonlinear stage of proton EMIC instability in the PIC simulation below.

3. Simulation

A standard periodic one-dimensional PIC simulation of a three-species plasma is performed. The system size is $L/(c/\omega_{\rm pp}) = 327.68$, where c is the speed of light and $\omega_{\rm pp}$ is the proton plasma frequency in the case of no α particles. The size of the spatial grid is the electron Debye length, while the number of super particles per cell for each species is 200. The ambient magnetic field is along the x-axis. The ratio of electron cyclotron frequency to plasma frequency is $\Omega_e/\omega_{pe} = 0.5$. The mass ratio of the three species is m_e:m_p:m_α = 1:25:100, where m_e, m_p, and m_α are the mass of electrons, protons, and α particles, respectively. The relative number density of the α particles to the electrons is $n_\alpha/n_e = 0.1$. Perpendicular proton beta is $\beta_{p\perp} = 0.2$, and proton temperature anisotropy is $T_{p\perp}/T_{p\parallel} = 100$. The temperature of α particles is isotropic and the same as that of the parallel proton temperature, $T_\alpha = T_{p\parallel}$. While the isotropic electron beta is $\beta_e = 0.08$, we confirmed that the following results are almost independent of electron beta. The proton temperature anisotropy is the only source of free energy in this system so that proton EMIC waves are the only waves that are linearly unstable.

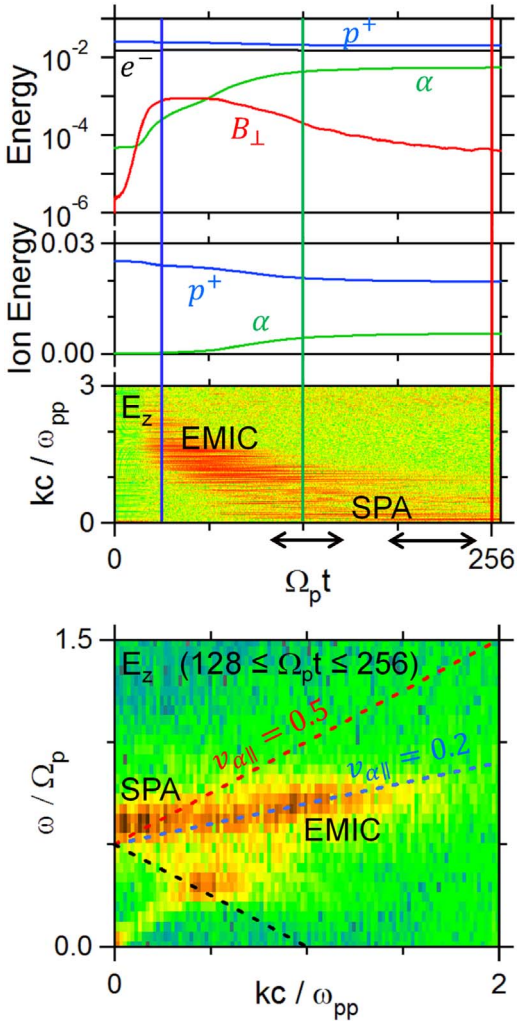

Figure 2. Time history of the PIC simulation. The first panel denotes energy time history of (p^+) protons, (e^-) electrons, (α) α particles, and ($B_\perp$) transverse magnetic field, respectively, in the logarithmic scale. The second panel shows only the energy of protons and α particles in the linear scale. The third panel indicates the time evolution of wavenumber spectrum of E_z component. The $\omega-k$ spectrum of E_z in the time interval of $128 \leqslant \Omega_p t \leqslant 256$ is shown in the fourth panel.

Figure 2 represents time evolution of energy (the first and the second panels) and wavenumber spectrum of E_z component (the third panel). The time is normalized to the inverse proton cyclotron frequency, Ω_p^{-1}. The rapid increase of the transverse magnetic field ($B_\perp$) energy is due to the proton EMIC instability. This leads to a relatively broadband spectrum of E_z component as well as the small increase of the α particle energy until the transverse magnetic field energy is saturated. After that, the energy of the α particles increases more and the spectral peak of the proton EMIC waves shifts to smaller wavenumbers. Furthermore, an additional spectral peak appears in very small wavenumbers, $kc/\omega_{\rm pp} \ll 1$. The amplified waves are the SPA waves. This is confirmed in the fourth panel in which the $\omega-k$ spectrum of the left-hand polarized fluctuations ($\omega > 0$) of the E_z component corresponding to the time interval of $128 \leqslant \Omega_p t \leqslant 256$ is depicted. Here, we have used the technique of Fourier decomposition to extract only the fluctuations with positive helicity ($k > 0$) and frequency ($\omega > 0$) from the original E_z data after Terasawa et al. (1986). Electron energy is almost unchanged throughout

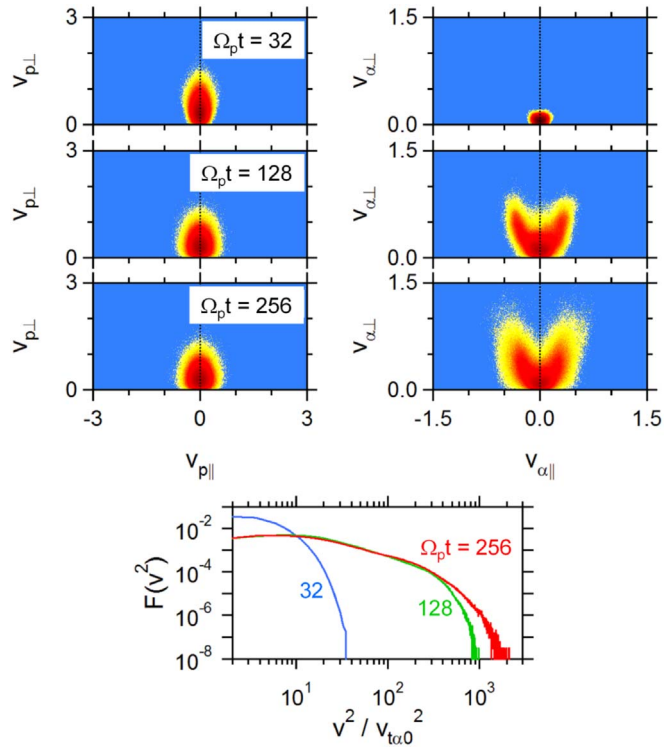

Figure 3. Evolution of velocity and energy distribution functions. The top three panels show velocity distribution functions of protons (left) and α particles (right) at $\Omega_p t = 32$, 128 and 256, respectively. The bottom panel denotes energy distribution functions of α particles at the corresponding times. The energy is normalized to initial thermal energy of the α particles.

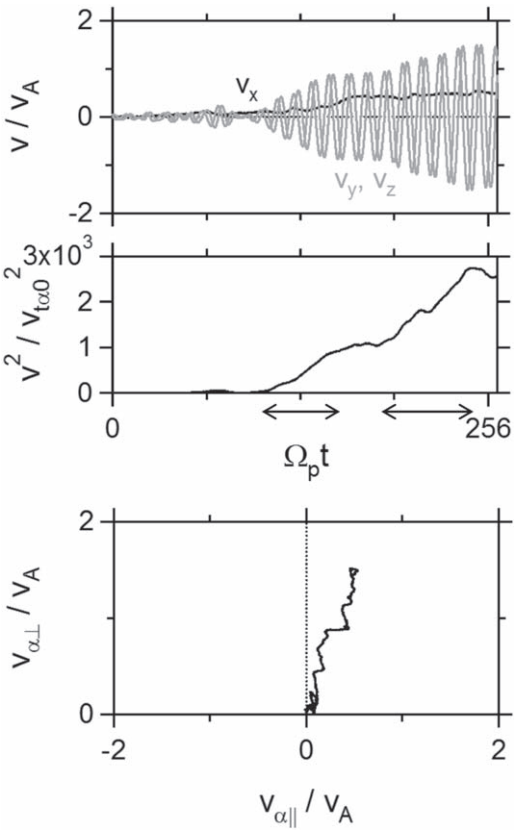

Figure 4. Trajectory of a nonthermal α particle. From the top, time evolution of three velocity components, that of energy, and the trajectory in velocity space are plotted. There are two main acceleration phases indicated by the horizontal arrows in the middle panel. The energy is normalized to the initial thermal energy of the α particles.

the run, indicating that they do not contribute to the process discussed above.

In Figure 3 the top three panels show velocity distribution functions of protons (left) and α particles (right) at three different times, $\Omega_p t = 32$, 128, and 256, indicated by the vertical lines in Figure 2. The velocities parallel and perpendicular to the ambient magnetic field are normalized to Alfvén velocity, v_A, in the case of no α particles. As time passes, the protons are isotropized and the α particles are accelerated to form a V-shaped distribution in the velocity space. Tanaka (1985) discussed this V-shaped velocity distribution of the α particles by using a hybrid simulation. He used the term "heating" instead of "acceleration" to express the V-shaped distribution. However, it is obvious from the bottom panel that the energy distribution function of the α particles indicates a nonthermal feature when the V-shaped velocity distribution is seen. Tanaka (1985) further interpreted this heating as a result of nonlinear interactions between the α particles and the proton EMIC waves.

Here, we focus on a trajectory of one of the well-accelerated nonthermal α particles. In Figure 4 the top and the middle panels show the time evolution of three components of velocity and that of energy. In the bottom panel a corresponding trajectory in velocity space is depicted. It is recognized in the middle panel that there are two acceleration phases. The first acceleration phase occurs in $105 \leqslant \Omega_p t \leqslant 155$, while the second phase occurs in $185 \leqslant \Omega_p t \leqslant 245$. The corresponding time domains are indicated by horizontal arrows in both Figures 4 and 2. In both acceleration phases this α particle gains energy mainly perpendicular to the ambient magnetic field as one can read from the top panel of Figure 4. In the first acceleration phase its parallel velocity is about $0.2v_A$ on average. The blue dashed line in the bottom panel of Figure 2 denotes the cyclotron resonance condition of the α particle ($\omega - kv_{\alpha\|} = \Omega_\alpha$) with its parallel velocity of $v_{\alpha\|} = 0.2v_A$. The line overlaps the region of the spectral peak amplified by the proton EMIC instability. Therefore, it is natural to conclude that the acceleration in the first phase is due to the interaction with the proton EMIC waves. After this first phase, the parallel velocity increases roughly to $0.5v_A$, probably through pitch angle scattering while its energy is not so changed. In the second acceleration phase the particle energy increases while this parallel velocity is almost kept constant. The corresponding resonance condition with $v_{\alpha\|} = 0.5v_A$ is also shown as the red dashed line in the bottom panel of Figure 2. It is indicated that this particle can resonate with the SPA waves. Since the wave spectrum is essentially symmetric with respect to k, the red line is folded back and indicated by the black dashed line. On this dashed line, there is another spectral peak around $kc/\omega_{pp} = 0.5$, which is due to another decay instability (Figure 1) on the α cyclotron branch. Hence, in this particular case the particle can resonate with the two kinds of nonlinearly generated waves, the SPA waves, and the α cyclotron waves, which is the same situation as discussed by Mizuta & Hoshino (2001).

4. Summary and Discussions

We proposed a mechanism of nonlinear generation of SPA waves in a three-component plasma, which is based on a

parametric instability of proton cyclotron waves generated by proton EMIC instability. The process was demonstrated self-consistently in a one-dimensional full PIC simulation. In the simulation not only the SPA waves but also the α cyclotron waves get excited. While protons lose their initial free energy and are isotropized, some α particles are accelerated to nonthermal energy. During its acceleration process, an α particle resonates simultaneously with the nonlinearly generated SPA waves and the α cyclotron waves. This is essentially the same situation as discussed by Mizuta & Hoshino (2001).

The generation of SPA waves in the nonlinear stage of the proton EMIC instability occurs in a wide parameter range. We confirmed that they are indeed generated even for smaller proton temperature anisotropy ($T_{p\perp}/T_{p\parallel} = 20$), smaller frequency ratio ($\Omega_e/\omega_{pe} = 0.1$), and for larger mass ratio (m_e:m_p:m_α = 1:100:400) cases.

In the current simulation α particles are energized first by interacting with the proton EMIC waves that have relatively lower phase velocities. Later, some of the energized particles resonate with both the nonlinearly generated SPA waves and the α cyclotron waves. Hence, the proton EMIC waves also play a role in injection, i.e., pre-acceleration of the α particles to be further able to resonate with the SPA as well as the α cyclotron waves. There may be other injection mechanisms. In this study the initial free energy of the system is provided only by the proton temperature anisotropy to make the scenario proposed here more visible. However, a situation where both protons and α particles have temperature anisotropy is also plausible. Since the temperature anisotropy of α particles results in the generation of α EMIC instability, some α particles can be resonantly accelerated by self-generated α EMIC waves so that they are injected into further interaction with the SPA waves. These α EMIC waves may also play an alternative role of the α cyclotron waves generated through a decay instability of proton EMIC waves.

Finally, we discuss the effect of relative α particle density, n_α/n_e, which may affect the dispersion property of the interacting waves as well as the acceleration of α particles. When n_α/n_e increases, proton density decreases so that free energy of the proton EMIC instability decreases even if proton temperature anisotropy is unchanged. This may suppress the acceleration of α particles. On the other hand, n_α/n_e influences the topology of the ω–k diagram. For instance, the cutoff frequency of the proton cyclotron branch increases with n_α/n_e. In such a case it is inferred from Figure 1 that the generated SPA wave has a higher phase velocity or equivalently stronger wave electric field. This may contribute to efficient acceleration of α particles. Hence, there may be the value of n_α/n_e leading to the highest efficiency of acceleration. To confirm this is a future issue.

We thank M. Hoshino, T. Amano, and Y. Matsumoto for fruitful discussions. S.M. acknowledges partial support by Grant-in-Aid for Scientific Research (C) No.19K03953 from JSPS.

ORCID iDs

S. Matsukiyo https://orcid.org/0000-0002-4784-0301

References

Aguilar, M., Aisa, D., Alpat, B., et al. 2015, ApJL, 808, L3
Davidson, R. C., & Ogden, J. M. 1975, PhFl, 18, 1045
Dayeh, M. A., Desai, M. I., Mason, G. M., Ebert, R. W., & Farahat, A. 2017, ApJ, 835, 155
Filwett, R. J., Desai, M. I., Dayeh, M. A., & Broiles, T. W. 2017, ApJ, 838, 23
Gary, S. P., Yin, L., & Winske, D. 2003, JGRA, 108, 1068
Gomberoff, L., Gratton, F., & Gnavi, G. 1995, JGR, 100, 1871
Gruesbeck, J. R., Lepri, S. T., Zurbuchen, T. H., & Christian, E. R. 2015, ApJ, 799, 57
Hollweg, J. V., & Isenberg, P. A. 2002, JGRA, 107, 1147
Horne, R. B., & Thorne, R. M. 1997, JGR, 102, 11457
Isenberg, P. A., Vasquez, B. J., & Hollweg, J. V. 2019, ApJ, 870, 119
Klecker, B., Möbius, E., & Popecki, M. A. 2007, SSRv, 130, 273
Kronberg, E. A., Ashour-Abdalla, M., Dandouras, I., et al. 2014, SSRv, 184, 173
Markovskii, S. A. 2007, ApJ, 666, 486
Mizuta, T., & Hoshino, M. 2001, GeoRL, 28, 3099
Reames, V. R. 2017, SoPh, 292, 156
Santos-Lima, R., de Gouveia Dal Pino, E. M., Kowal, G., et al. 2014, ApJ, 781, 84
Sckopke, N., Paschmann, G., Bame, S. J., & Gosling, J. T. 1983, JGR, 88, 6121
Shevchenko, V., Galinsky, V., & Winske, D. 2006, GeoRL, 33, L23101
Shimada, N., & Hoshino, M. 2005, JGRA, 110, A02105
Tanaka, M. 1985, JGR, 90, 6459
Terasawa, T., Hoshino, M., Sakai, J.-I., & Hada, T. 1986, JGR, 91, 4171
Thorne, R. M., & Horne, R. B. 1993, GeoRL, 20, 317
Thorne, R. M., & Horne, R. B. 1994, JGR, 99, 17275
Tu, C.-Y., Wang, L.-H., & Marsch, E. 2003, JGRA, 108, 1161
Wang, Z., Sun, K., Zhang, Y., & Zhai, H. 2019, PhPl, 26, 022903